An ε-uniform Finite Element Method for Singularly Perturbed Boundary Value Problems

Q. S. Song[*]　　　　G. Yin[†]　　　　Z. Zhang[‡]

February 2, 2008

Abstract

This work develops an ε-uniform finite element method for singularly perturbed boundary value problems. A surprising and remarkable observation is illustrated: By moving one node arbitrarily in between its adjacent nodes, the new finite element solution always intersect with original one at fixed point. Using this fact, an effective ε-uniform approximation out of boundary is proposed by adding one point only in the grid that contains boundary layer. The thickness of boundary layer is not necessary to be known from *priori estimation*. Numerical results are carried out and compared to Shishkin mesh for demonstration purpose.

Key Words. finite element method, singular perturbation, ε-uniform approximation, layer-adapted mesh, Shishkin mesh.

Mathematics Subject Classification.

Brief Title. An ε-uniform Approximation of Singularly Perturbed BVP

[*]Department of Mathematics, Wayne State University, Detroit, MI 48202, `song@math.wayne.edu`. Research of this authors was supported in part by a WSU graduate research assistantship.

[†]Department of Mathematics, Wayne State University, Detroit, MI 48202, `gyin@math.wayne.edu`. Research of this author was supported in part by the National Science Foundation, and in part by Wayne State University Research Enhancement Program.

[‡]Department of Mathematics, Wayne State University, Detroit, MI 48202, `zzhang@math.wayne.edu`. Research of this author was supported in part by the National Science Foundation, and in part by Michigan Life Science Corridor.

1   Introduction

This paper is concerned with linear Galerkin finite element method for singularly perturbed boundary value problems (BVPs). Consider an one-dimensional BVP problem

$$-\varepsilon u'' - bu' + cu = f, \quad u(0) = u(1) = 0, \quad x \in [0,1]. \tag{1}$$

For simplicity, let $b \leq 0, c \geq 0$, and $0 < \varepsilon \ll 1$ are constant such that not both b and c are 0. If $b > 0$, by using substitution $w(x) = u(1-x)$, it reduces to the case with $b \leq 0$. If $b = 0, c > 0$, equation (1) is said to be a reaction diffusion equation. If $b < 0, c = 0$, equation (1) is the so-called convection diffusion equation. All the results presented in this paper can be readily generalized to smooth and non-vanishing functions of $b(x)$ and $c(x)$.

If the exact solution $u(\cdot)$ of (1) is "bad" in the sense that $\|u''\|_\infty$ is not bounded uniformly in ε, the standard finite element method (FEM) generates huge errors through the whole domain. Typically, it is caused by a small interval of width $O(\varepsilon)$ (called boundary layer), in which u'' rapidly changes.

To overcome the difficulties in the singular perturbation, it is desirable to put more grid points near the boundary layer or stablize the appoximation methods. Streamline diffusion finite element methods (SDFEM), upwinding FEM, Bakhalov grid, Shishkin grid, and many other such schemes are extensively studied in the context of singularly purturbed problems since 1970s, see [11, 9, 4, 8, 14, 1]. Among them, Shishkin grid became popular due to its simple structure and high accuracy. The Shishkin mesh was first introduced in finite difference methods and has been discussed in [8]; the reader is referred to a survey article [13] for further details. A typical Shishkin mesh is to construct $n+n$ grid, which is indeed n uniform grids in boundary layer plus n uniform grids out of boundary layer. By this method, the approximation provides ε-uniform accuracy. But they require *a priori* estimation in order to determine the thickness of the bounded layer. On the other hand, it makes error analysis more complicated, since the errors from boundary layer affect the solution in the entire domain. Therefore, if an approximation can be stabilized and ε-uniform by simply adding one point to original n grid, it deserves to be worked out.

In this work, we focus on FEM solutions of (1) by starting with an interesting observation. Given a grid $\mathcal{T}^n = \{0 = x_0 < \cdots < x_n < x_{n+1} = 1\}$, we add m points arbitrarily in $[x_n, 1]$, denoted by $\mathcal{T}^{n+m}$. Then FEM solutions on $\mathcal{T}^n$ and $\mathcal{T}^{n+m}$ intersect each other at a fixed point in each interval of out of boundary layer, that is, the locations of intersection

in each interval is indpendent of m and the distribution of added points, see Figure 1-a, Figure 3-a, and Figure 4. This directly implies that the accuracy on those intersections are as good as FEM solutions on the grid $\mathcal{T}^{n+m}$ by choosing $m \to \infty$, denoted by $\mathcal{T}^{n+\infty}$. Provided that the boundary layer is covered by $[x_n, 1]$, the above observation gives the start point of ε-uniform approximation. In lieu of interpolating these intersections, we present a better way to obtain an ε-uniform approximation. By adding one point $\hat{s}_1 \in (x_n, 1)$ with $|\hat{s}_1 - x_n| = O(\varepsilon)$ or $|\hat{s}_1 - x_n| = O(\sqrt{\varepsilon})$, the interval $[x_n, \hat{s}_1]$ block the error impact from boundary layer completely. The theoretical result shows that the FEM solutions with grid $\mathcal{T}^n \cup \{\hat{s}_1\}$ in $[0, x_n]$ is the same as the FEM solution of

$$-\varepsilon w'' - bw' + cw = f, \quad w(0) = 0, \ w(\hat{s}_1) = u(\hat{s}_1), \quad x \in [0, \hat{s}_1], \tag{2}$$

where $u(\hat{s}_1)$ is exact solution at the point of $\hat{s}_1$, and $w''(\cdot)$ is uniformly bounded. This enables us to use all kinds of standard FEM error analysis in $[0, \hat{s}_1]$, no matter how huge errors are generated in $[\hat{s}_1, 1]$. Therefore, the FEM errors in $[0, x_n]$ has the accuracy of $\mathcal{T}^{n+1+\infty}$, which is clearly better than Shishkin mesh $\mathcal{T}^{n+n}$ in both accuracy and computing cost. Another advantage is: One need not know the thickness of boundary layer, since $\hat{s}_1$ is not necessarily in boundary layer.

The rest of this paper is arranged as follows. Section 2 begins with the model and notation. Section 3 proceeds with the observation on intersections of a family of FEM solutions. Section 4 presents an ε-uniform FEM, which can isolate the boundary layer. Some auxiliary results are included in Section 5. Section 6 displays some numerical experiment results, including solutions of convection-diffusion equation, reaction-diffusion equation, and Green function. Finally, we close this paper with further remarks.

2 Formulation

Let $H^1 = \{v, v' \in L^2\}$, and $H_0^1 = \{v | v \in H^1, v(0) = v(1) = 0\}$. The weak solution of (1) is a function $u \in H_0^1$, satisfying

$$a(u, v) = (f, v), \forall v \in H_0^1, \tag{3}$$

where $(\cdot, \cdot)$ is L^2 inner product, and $a(u, v) = \varepsilon(u', v') + b(u, v') + c(u, v)$.

For a positive integer $n \geq 2$, let $\mathcal{T}^n$ be an arbitrary grid of the form

$$\mathcal{T}^n = \{x_i | 0 = x_0 < x_1 < \cdots < x_{n+1} = 1\}, \tag{4}$$

3

and let $h_i = x_i - x_{i-1}$. By $\phi_i(x)$, we denote the nodal basis function at x_i for $1 \leq i \leq N$ by

$$\phi_i(x) = \begin{cases} \dfrac{x - x_{i-1}}{h_i} & \text{if} \quad x \in [x_{i-1}, x_i] \\ \dfrac{x_{i+1} - x}{h_{i+1}} & \text{if} \quad x \in [x_i, x_{i+1}] \\ 0 & \text{otherwise.} \end{cases} \tag{5}$$

The finite element space is defined by $V^n = \{v^n | v^n = \sum_{i=1}^{n} v_i^n \phi_i(x)\}$. The finite element discretization of (3) is to find $u^n \in V^n$ such that

$$a(u^n, v^n) = (f, v^n), \forall v^n \in V^n \cap H_0^1. \tag{6}$$

Existence and uniqueness of u^n can be found in [2] and references therein. Now we denote

$$u^n = \sum_{i=1}^{n} u_i^n \phi_i. \tag{7}$$

Rewrite (6) as

$$\sum_{i=1}^{n} u_i^n a(\phi_i, \phi_j) = (f, \phi_j), j = 1, 2, \ldots n. \tag{8}$$

Let A be an $n \times n$ matrix with

$$a_{ij} = a(\phi_j, \phi_i). \tag{9}$$

Detailed calculation leads to further specific form of

$$\begin{aligned} a_{i,i} &= \varepsilon\left(\frac{1}{h_i} + \frac{1}{h_{i+1}}\right) + \frac{c}{3}(h_i + h_{i+1}) \\ a_{i,i-1} &= -\frac{\varepsilon}{h_i} + \frac{b}{2} + \frac{c}{6}h_i \\ a_{i,i+1} &= -\frac{\varepsilon}{h_{i+1}} - \frac{b}{2} + \frac{c}{6}h_i \\ a_{i,j} &= 0, \quad \text{if } |i - j| \geq 2 \end{aligned} \tag{10}$$

Let $U^n = (u_1^n, \ldots, u_n^n)'$ and $F = ((f, \phi_1), \ldots, (f, \phi_n))'$ be column vectors. Then, (8) is equivalent to the linear system of equations

$$AU^n = F. \tag{11}$$

Typically a FEM solution of a singularly perturbed BVP problem has boundary layer in a small interval (associated with ε) of rapid variations of u''. Throughout this paper, unless it's explicitly mentioned, we assume solution u of (1) has a boundary layer at $x = 1$ and x_n

4

is located outside the boundary layer. This is reasonable assumption due to the very short interval of boundary layer depending on $0 < \varepsilon \ll 1$. All the results below can be obtained analogously for any boundary layer located in $[0, 1]$.

Let $\mathcal{T}^{n+m} = \mathcal{T}^n \cup \{s_1, \ldots, s_m\}$, where $x_n < s_1 < \cdots < s_m < x_{n+1}$. Denote the nodal basis functions on $\mathcal{T}^{n+m}$ by $\{\phi_1, \ldots, \phi_{n-1}, \widetilde{\phi}_n, \phi_{s_1}, \ldots, \phi_{s_m}\}$, where $\widetilde{\phi}_n$ and ϕ_{s_i} are nodal basis for x_n and s_i, respectively. Note that the first $n - 1$ nodal basis functions of $\mathcal{T}^{n+m}$ are exactly the same as those of $\mathcal{T}^n$. Let V^{n+m} be the function space with basis $\{\phi_1, \ldots, \phi_{n-1}, \widetilde{\phi}_n, \phi_{s_1}, \ldots, \phi_{s_m}\}$. It is obvious that $V^n \subset V^{n+m}$. Write u^{n+m}, the FEM solution of (1) in V^{n+m}, as

$$u^{n+m} = \sum_{i=1}^{n-1} u_i^{n+m} \phi_i + u_n^{n+m} \widetilde{\phi}_n + \sum_{i=1}^{m} u_{s_i}^{n+m} \phi_{s_i}. \tag{12}$$

In the next section, we fix $\mathcal{T}^n$, and start with observation on the intersections of u^n and u^{n+m} for different $\mathcal{T}^{n+m}$. For convenience, we use $Q_i \in u^n \cap u^{n+m}$ to denote the intersetion of u^n and u^{n+m} in the interval (x_{i-1}, x_i), and by $x(Q_i)$ and $y(Q_i)$ we denote x- and y- coordinate of Q_i respectively. The result shows that the intersections $\{Q_i : 2 \leq i \leq n\}$ are independent of m and distribution of s_i. Therefore, by adding only one point $\{s_1\}$, we can compute $\{Q_i \in u^n \cap u^{n+1}\}$, and the accuracy of Q_i has the same accuracy as $u^{n+\infty}$.

3 Intersections of u^n and u^{n+m}

Theorem 3.1. Fix $\mathcal{T}^n$. By adding one point $s_1 \in (x_n, 1)$ arbitrarily, we obtain new grid $\mathcal{T}^{n+1}$. Then the intersection Q_i of u^n and u^{n+1} in the interval (x_{i-1}, x_i) is independent of the choice of s_1 for any $i = 2, 3, \ldots, n$. That is, those coordinates of intersections do not depend on the choice of $s_1 \in (x_n, x_{n+1})$.

Proof. Analogous to (8), we have a system of linear equations with respect to $\{u_i^{n+1}, i = 1, \ldots, n; u_{s_1}^{n+1}\}$, given by

$$\sum_{i=1}^{n-1} u_i^{n+1} a(\phi_i, \phi_j) + u_n^{n+1} a(\widetilde{\phi}_n, \phi_j) + u_{s_1}^{n+1} a(\phi_{s_1}, \phi_j) = (f, \phi_j), \quad j = 1, 2, \ldots, n-1, \tag{13}$$

$$\sum_{i=1}^{n-1} u_i^{n+1} a(\phi_i, \widetilde{\phi}_n) + u_n^{n+1} a(\widetilde{\phi}_n, \widetilde{\phi}_n) + u_{s_1}^{n+1} a(\phi_{s_1}, \widetilde{\phi}_n) = (f, \widetilde{\phi}_n), \tag{14}$$

5

and

$$\sum_{i=1}^{n-1} u_i^{n+1} a(\phi_i, \phi_{s_1}) + u_n^{n+1} a(\widetilde{\phi}_n, \phi_{s_1}) + u_{s_1}^{n+1} a(\phi_{s_1}, \phi_{s_1}) = (f, \phi_{s_1}), \tag{15}$$

Note that for $1 \le j \le n-1$, $a(\widetilde{\phi}_n, \phi_j) = a(\phi_n, \phi_j)$ and $a(\phi_{s_1}, \phi_j) = 0$, and (13) leads to

$$\sum_{i=1}^{n} u_i^{n+1} a(\phi_i, \phi_j) = (f, \phi_j), \quad j = 1, 2, \ldots, n-1. \tag{16}$$

On the other hand, for $1 \le i \le n-1$, $a(\phi_i, \widetilde{\phi}_n) = a(\phi_i, \phi_n)$, and (14) yields

$$\sum_{i=1}^{n-1} u_i^{n+1} a(\phi_i, \phi_n) + u_n^{n+1} a(\widetilde{\phi}_n, \widetilde{\phi}_n) = (f, \widetilde{\phi}_n) - u_{s_1}^{n+1} a(\phi_{s_1}, \widetilde{\phi}_n). \tag{17}$$

For $1 \le i \le n-1$, $a(\phi_i, \phi_{s_1}) = 0$, so it follows from (15)

$$u_n^{n+1} a(\widetilde{\phi}_n, \phi_{s_1}) = (f, \phi_{s_1}) - u_{s_1}^{n+1} a(\phi_{s_1}, \phi_{s_1}). \tag{18}$$

Let $p = (1-s)/h_{n+1}$. Observe $\phi_n = \widetilde{\phi}_n + p\phi_{s_1}$. Combining two equations above according to (17)+p*(18), we have

$$\sum_{i=1}^{n-1} u_i^{n+1} a(\phi_i, \phi_n) + u_n^{n+1} a(\widetilde{\phi}_n, \phi_n) = (f, \phi_n) - u_{s_1}^{n+1} a(\phi_{s_1}, \phi_n). \tag{19}$$

Hence,

$$\sum_{i=1}^{n} u_i^{n+1} a(\phi_i, \phi_n) = (f, \phi_n) - u_{s_1}^{n+1} a(\phi_{s_1}, \phi_n) + p u_n^{n+1} a(\phi_{s_1}, \phi_n). \tag{20}$$

Let $U^{n+1} = (u_1^{n+1}, \ldots, u_n^{n+1})'$ be a column vector with length n. By (16) and (20),

$$A U^{n+1} = \widetilde{F}, \tag{21}$$

where $\widetilde{F}$ is a column vector with left-hand side of (16) and (20) as elements. Subtracting (21) from (11),

$$A(U^n - U^{n+1}) = F - \widetilde{F} \tag{22}$$

Notice that $F - \widetilde{F} = C_{s,1} e_n$, where $e_n = (0, \ldots, 0, 1)'$ is a vector with length n, and $C_{s,1} = u_{s_1}^{n+1} a(\phi_{s_1}, \phi_n) - p u_n^{n+1} a(\phi_{s_1}, \phi_n)$. Note that $C_{s,1}$ is a scalar depending only on s_1, since u_n^{n+1} term in $C_{s,1}$ is completely determined by s_1. Therefore,

$$U^n - U^{n+1} = C_{s,1} A^{-1} e_n \tag{23}$$

The last equation tells us every $u_i^n - u_i^{n+1}$ increases or decreases by the factor $C_{s,1}$ uniformly in i. Using elementary similar triangle properties, we prove the result. $\qquad \square$

6

Remark 3.2. If $u_i^n - u_i^{n+1}$ and $u_{i+1}^n - u_{i+1}^{n+1}$ have opposite sign, then u^n and u^{n+1} have intersection in (x_i, x_{i+1}). Notice that $A^{-1}e_n$ in (23) is FEM solution of green function of operator A. It is very common that FEM solution of green function intersects x-axis in each grid. Intuitively, this explains why u^n and u^{n+1} intersect each other in every grid in most cases. Later we will present the criteria to be used for identifying the existence of intersections, see Lemma 5.1. Moreover, if there is no intersection in some interval (x_i, x_{i+1}) for a choice of s_1, then there will be no intersection for any choice of s_1.

Theorem 3.3. Fix $\mathcal{T}^n$. Let $\mathcal{T}^{n+m} = \mathcal{T}^n \cup \{s_1 < s_2 < \cdots < s_m\}$, where $s_i \in (x_n, 1)$. Then the intersection Q_i of u^n and u^{n+m} in the interval (x_{i-1}, x_i) is independent of m and distribution of $\{s_i\}$ for any $i = 2, 3, \ldots, n$.

Proof. Let V^{n+m} be a function space with nodal basis functions $\{\phi_1, \ldots, \phi_{n-1}, \widetilde{\phi}_n, \phi_{s_1}, \ldots, \phi_{s_m}\}$ on $\mathcal{T}_{n+m}$. Analogous to (16), we have

$$\sum_{i=1}^{n} u_i^{n+m} a(\phi_i, \phi_j) = (f, \phi_j), \quad j = 1, 2, \ldots, n-1. \tag{24}$$

Since $V^{n+m} \supset V^n$, there exists a linear combination $\phi_n = \widetilde{\phi}_n + \sum_{i=1}^{m} p_i \widetilde{\phi}_{s_i}$ for some $p_1, p_2, \ldots, p_m \in [0, 1]$. Applying similar arguments as that of Theorem 3.1, we obtain

$$\sum_{i=1}^{n} u_i^{n+m} a(\phi_i, \phi_n) = (f, \phi_n) + \sum_{i=1}^{m} (p_i u_n^{n+m} - u_{s_i}^{n+m}) a(\phi_{s_i}, \phi_n). \tag{25}$$

Define $C_{s,m} = \sum_{i=1}^{m} (u_{s_i}^{n+m} - p_i u_n^{n+m}) a(\phi_{s_i}, \phi_n)$. Using exactly the same argument in (23), we have

$$U^n - U^{n+m} = C_{s,m} A^{-1} e_n. \tag{26}$$

Hence, the result follows. $\quad\square$

Corollary 3.4. Fix $\mathcal{T}^n$. Let $\mathcal{T}^{n+m} = \mathcal{T}^n \cup \{s_1 < s_2 < \cdots < s_m\}$, where $s_i \in (0, x_1)$. Then the intersection Q_i of u^n and u^{n+m} in the interval (x_{i-1}, x_i) is independent of m and distribution of $\{s_i\}$ fixed for any $i = 2, \ldots, n$.

Proof. We rearrange the order of the index from $\{0, 1, 2, \ldots, n, n+1\}$ to $\{n+1, n, \ldots, 1, 0\}$, and change the coordinate linearly from $[0, 1]$ into $[1, 0]$. Using the same line of argument as that of Theorem 3.3, the result holds. $\quad\square$

Corollary 3.5. Fix $\mathcal{T}^n$. Let $\mathcal{T}^{n+m} = \mathcal{T}^n \cup \{s_1 < s_2 < \cdots < s_m\}$, where $s_i \in (x_{k-1}, x_k)$ for some $2 \leq k \leq n$. Then the intersection of u^n and u^{n+m} in the interval (x_{i-1}, x_i) is independent of m and distribution of $\{s_i\}$ for any $i \in \{2, \ldots, n\} \setminus \{k\}$.

Proof. This is straight forward result from Theorem 3.3 and Corollary 3.4. $\square$

4 An ε-uniform Approximation u^{n+1} in $[0, x_n]$

In the previous section, by arbitrarily choosing a point $s_1 \in (x_n, 1)$, we can determine $Q_i \in u^n \cap u^{n+1}$ in each interval, and the result shows Q_i has the same accuracy as that of $u^{n+\infty}$. In this section, by choosing appropriate $\hat{s}_1 \in (x_n, 1)$, we obtain $\hat{u}^{n+1}$, which has ε-uniform accuracy in $[0, x_n]$. This will automatically imply that Q_i has ε-uniform accuracy, since $Q_i \in \hat{u}^{n+1}$. For simplicity, we slightly abuse notation: Let $a_{n,\hat{s}_i} = a(\phi_{\hat{s}_i}, \phi_n)$ without confusing.

Lemma 4.1. There exists $\hat{s}_1 \in (x_n, 1)$, such that, $a_{n,\hat{s}_1} = 0$ for $\hat{\mathcal{T}}^{n+1} = \{x_0 < x_1 < \cdots < x_n < \hat{s}_1 < x_{n+1}\}$.

Proof. By (10), to establish the desired result, it is equivalent to prove that there exists $0 < h_{\hat{s}_1} < 1 - x_n$, satisfies

$$-\frac{\varepsilon}{\hat{s}_1} - \frac{b}{2} + \frac{c}{6}h_{\hat{s}_1} = 0, \tag{27}$$

where $h_{\hat{s}_1} = \hat{s}_1 - x_n$. By eliminating the denominators in the equation (27), we have

$$ch_{\hat{s}_1}^2 - 3bh_{\hat{s}_1} - 6\varepsilon = 0. \tag{28}$$

If $c = 0$, then $b < 0$, and $h_{\hat{s}_1} = \dfrac{-2\varepsilon}{b} > 0$. If $c \neq 0$, then the determinant of (28) is $9b^2 + 24\varepsilon c > 0$. Write $h_{\hat{s}_1}$ using quadratic formula,

$$0 < h_{\hat{s}_1} = \frac{3b + \sqrt{9b^2 + 24\varepsilon c}}{2c} \leq \sqrt{\frac{6\varepsilon}{c}}. \tag{29}$$

Thus, $h_{\hat{s}_1} = O(\varepsilon)$ if $c = 0$, and $h_{\hat{s}_1} = O(\sqrt{\varepsilon})$ if $c \neq 0$. $\square$

Remark 4.2. The essence of Lemma 4.1 is to find such a $h_{\hat{s}_1}$ with $a_{n,\hat{s}_1} = 0$. If b and c are not constant, we can compute the formula for $h_{\hat{s}_1}$ involved with integrals. It is also possible to find it by discretizations.

8

Theorem 4.3. Given $\mathcal{T}^n$, take $\hat{\mathcal{T}}^{n+1}$ and $\hat{s}_1$ as in Lemma 4.1. Use $\hat{u}^{n+1}$ to denote the FEM solution on $\mathcal{T}^{n+1}$ of (1). Consider another BVP problem

$$-\varepsilon w'' - bw' + cw = f, \quad w(0) = 0, w(\hat{s}_1) = u(\hat{s}_1), \tag{30}$$

where $u(\cdot)$ is solution of (1). Use w^n to denote the FEM solution of (30) on $\hat{\mathcal{T}}^{n+1} \setminus \{1\}$, then

$$w(x) = u(x), \quad \forall x \in [0, \hat{s}_1], \tag{31}$$

and

$$\hat{u}^{n+1}(x) = w^n(x), \quad \forall x \in [0, x_n]. \tag{32}$$

Proof. Note that $(\hat{u}_1^{n+1}, \hat{u}_2^{n+1}, \ldots, \hat{u}_n^{n+1})$ is a solution of the system of linear equations

$$\begin{cases} a_{i,i-1}\hat{u}_{i-1}^{n+1} + a_{i,i}\hat{u}_i^{n+1} + a_{i,i+1}\hat{u}_{i+1}^{n+1} = (f, \phi_i) & i = 1, 2, \ldots, n-1 \\ a_{n,n-1}\hat{u}_{n-1}^{n+1} + a_{n,n}\hat{u}_n^{n+1} = (f, \widetilde{\phi}_n) - a_{n,\hat{s}_1}\hat{u}_{\hat{s}_1}^{n+1}. \end{cases} \tag{33}$$

Let $w^n = \sum_{i=1}^{n-1} w_i^n \phi_i + w_n^n \widetilde{\phi}_n + w_{\hat{s}_1}^n \phi_{\hat{s}_1}^-$, where $\phi_{\hat{s}_1}^- = \phi_{\hat{s}_1}|_{[0,\hat{s}_1]}$. Then $(w_i^n$ for $i \in \{1, 2, \ldots, n, \hat{s}_1\})$ is a solution of the system of linear equations

$$\begin{cases} a_{i,i-1}w_{i-1}^n + a_{i,i}w_i^n + a_{i,i+1}w_{i+1}^n = (f, \phi_i) & i = 1, 2, \ldots, n-1 \\ a_{n,n-1}w_{n-1}^n + a_{n,n}w_n^n = (f, \widetilde{\phi}_n) - a_{n,\hat{s}_1}w_{\hat{s}_1}^n \\ w_{\hat{s}_1}^n = u(\hat{s}_1). \end{cases} \tag{34}$$

The solutions of (33) and (34) are precisely the same, since $a_{n,\hat{s}_1} = 0$. □

Remark 4.4. From Theorem 4.3, we can separate the boundary layer by adding point $\hat{s}_1 \in (x_n, 1)$. Therefore, it is equivalent to solve non-singularly perturbed BVP problems by the FEM, and all general FEM error analysis works well without effected by boundary layer. For example, if $\{0 < x_1 < \cdots < x_n\}$ is uniform mesh in $[0, x_n]$, then $\|\hat{u}^{n+1}\|_{\infty, [0,x_n]}$ is bounded by $\|u''\|_{\infty, [0, x_n + O(\sqrt{\varepsilon})]} h^2$, and $\|u''\|_{\infty, [0, x_n + O(\sqrt{\varepsilon})]}$ is ε-uniformly bounded. On the other hand, add m points in $(\hat{s}_1, 1)$, denoted by $\hat{\mathcal{T}}^{n+1+m}$. Use $\hat{\mathcal{T}}^{n+1+\infty}$ to denote the grid which is almost dense in $[\hat{s}_1, 1]$. Use $\hat{u}^{n+1+\infty}$ to denote the FEM solution of (1) on $\hat{\mathcal{T}}^{n+1+\infty}$. Then, $\hat{u}^{n+1}$ is exactly the same with $\hat{u}^{n+1+\infty}$ on $[0, x_n]$.

5 Auxiliary results

Recall A is an $n \times n$ matrix with $a_{ij} = a(\phi_j, \phi_i)$, and e_n is $(0, \ldots, 0, 1)'$ of length n. Let A_i be matrix replacing ith column of A with e_n.

Lemma 5.1. Fix $\mathcal{T}^n$. Let $\mathcal{T}^{n+m} = \mathcal{T}^n \cup \{s_1 < s_2 < \cdots < s_m\}$, where $s_i \in (x_n, x_{n+1})$. Then u^n and u^{n+m} have their intersection Q_i in the interval (x_{i-1}, x_i) for some $2 \leq i \leq n$ if and only if

$$\det[A_i A_{i-1}] < 0, \tag{35}$$

and the coordinates of Q_i is given by

$$Q_i = \left(\frac{r_i}{r_i + 1} x_i + \frac{1}{r_i + 1} x_{i-1}, \frac{r_i}{r_i + 1} u_i^n + \frac{1}{r_i + 1} u_{i-1}^n \right), \tag{36}$$

where $r_i = |\det A_{i-1} / \det A_i|$.

Proof. To obtain Q_i, we apply $\mathcal{T}^n$ and $\mathcal{T}^{n+m}$ to Theorem 3.3. Using Crammer's rule in (26), we obtain

$$u_i^n - u_i^{n+m} = C_{s,m} \frac{\det A_i}{\det A}, \quad i = 1, 2, \ldots, n, \tag{37}$$

Therefore

$$\frac{u_i^n - u_i^{n+m}}{u_{i-1}^n - u_{i-1}^{n+m}} = \frac{\det A_i}{\det A_{i-1}}, \quad i = 2, \ldots, n. \tag{38}$$

A necessary and sufficient condition to have an intersection is $(u_i^n - u_i^{n+m})/(u_{i+1}^n - u_{i+1}^{n+m}) < 0$. This proves (35). Using similar triangles, (36) follows. $\qquad\square$

It is very common to have oscillation in finite element solution, and we can use Lemma 5.1 to verify its behavior, see Remark 3.2. The following theorem is a direct consequence of using Shishkin mesh.

Theorem 5.2. Assume $\mathcal{T}^n$ is a uniform grid in $[0, 1]$ satisfies condition (35), and the boundary layer is at $x = 1$. Then

$$\max_{1 \leq i \leq n-1} |u^n(x(Q_i)) - u_I^n(x(Q_i))| < Cn^{-2}, \tag{39}$$

where C is independent of ε.

Proof. We put $m = O(n)$ grid in $(x_n, 1)$, so that $\mathcal{T}^{n+m}$ forms Bakhvalov grid or Shishkin grid. The uniform convergence of u^{n+m} on $\mathcal{T}^{n+m}$ is well known (see [5, 7, 8, 15]) as

$$\|u^{n+m} - u_I^{n+m}\|_\infty \leq Cn^{-2} \tag{40}$$

Also, we have $Q_i \in u^{n+m} \cap u^n$ by Corollary 3.5. So

$$|u^{n+m}(x(Q_i)) - u_I^{n+m}(x(Q_i))| \leq Cn^{-2}. \tag{41}$$

Note that $u_I^{n+m}|_{(0,x_n)} = u_I^n|_{(0,x_n)}$. Thus, the theorem holds. $\qquad\square$

10

Remark 5.3. From the result of Theorem 5.2, we have estimation of $O(h^2)$. In non-uniform case, we can obtain an error bound $O(h)$ directly from [3].

6   Numerical Results

In this section, we present several examples.The first is a convection diffusion equation, the second is a reaction diffusion equation, and the last one is a Green function.

Example 6.1. Consider the convection-diffusion equation:

$$-\varepsilon u'' + u' = x, \quad u(0) = u(1) = 0. \tag{42}$$

The exact solution is

$$u = x\left(\frac{x}{2} + \varepsilon\right) - \left(\frac{1}{2} + \varepsilon\right)\left(\frac{e^{(x-1)/\varepsilon} - e^{-1/\varepsilon}}{1 - e^{-1/\varepsilon}}\right). \tag{43}$$

The solution $u(\cdot)$ has a boundary layer at $x = 1$, and is nearly quadratic outside the boundary layer.

First, we use the linear finite element method on two different grid $\mathcal{T}^{15}$ and $\mathcal{T}^{15+1}$ for $\varepsilon = 10^{-3}$, where $\mathcal{T}^{15}$ is a uniform mesh on $[0,1]$ with 16 intervals, and $\mathcal{T}^{15+1}$ is a modified $\mathcal{T}^{15}$ with one point added at the center of the last interval. The intersections of finite element solution u^{15} and u^{15+1} are almost on the interpolation of exact solution u_I^{15+1}, as shown in Figure 1-a.

Second, we use the grid $\hat{\mathcal{T}}^{15+1}$ to compute for the same ε, where $\hat{\mathcal{T}}^{15+1}$ is modified from $\mathcal{T}^{15}$ by adding one specific point $\hat{s}_1 \in (x_n, 1)$ with $\hat{s}_1 - x_n = 2\varepsilon$, see Lemma 4.1. The finite element solution $\hat{u}^{15+1}$ is almost overlapped with interpolation of interpolation of exact solution u_I^{15} in $[0, x_n]$, as seen from Figure 1-b. This verifies Theorem 4.3.

To compare with the well-known Shishkin mesh, we construct $\mathcal{T}_s^{n+n}$, which divides both $[0, 1-\theta]$ and $[1-\theta, 1]$ into n equidistant subintervals, where $\theta = \{\frac{1}{2}, \frac{2\varepsilon \ln 2n}{b}\}$. u_s^{n+n} is used to denote the FEM solution on $\mathcal{T}_s^{n+n}$. Table 1 shows the maximum norm of $u_I^{n+1} - \hat{u}^{n+1}$ and $u_I^{n+1} - u_s^{n+n}$ in $[0, x_n]$. Apparently, both $\hat{u}^{n+1}$ and u_s^{n+n} has ε-uniform accuracy. However, $\hat{u}^{n+1}$ has better accuracy than u_s^{n+n} by using less grids. The reason is that $\hat{u}^{n+1}$ is completely isolated from the impact of errors from boundary layer; see Table 1. This also verifies Theorem 4.3.
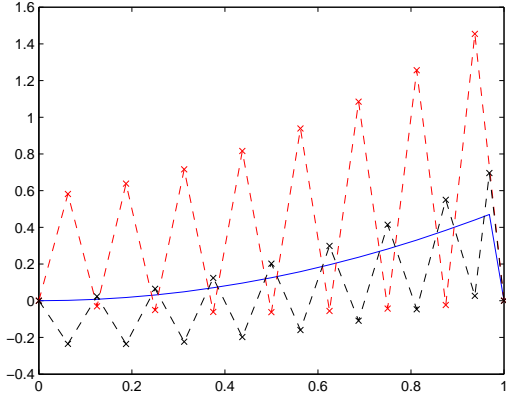
(a) u^{15} and u^{15+1}(dotted lines); u_I^{15+1}(solid line)
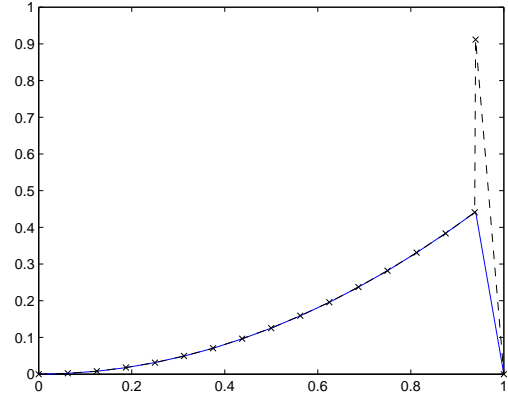
(b) $\hat{u}^{15+1}$(dotted line) and u_I^{15} (solid line)

Figure 1: FEMs with $\varepsilon = 10^{-3}$ for Example 6.1

	$\varepsilon = 10^{-5}$		$\varepsilon = 10^{-10}$	
n	$\|u_I^{n+1} - \hat{u}^{n+1}\|_{\infty,[0,x_n]}$	$\|u_I^{n+1} - u_s^{n+n}\|_{\infty,[0,x_n]}$	$\|u_I^{n+1} - \hat{u}^{n+1}\|_{\infty,[0,x_n]}$	$\|u_I^{n+1} - u_s^{n+n}\|_{\infty,[0,x_n]}$
4	6.663e-003	1.117e-002	6.667e-003	1.117e-002
8	2.054e-003	1.567e-003	2.058e-003	1.569e-003
16	5.734e-004	3.480e-004	5.767e-004	3.500e-004
32	1.498e-004	8.384e-005	1.530e-004	8.569e-005
64	3.637e-005	1.948e-005	3.941e-005	2.115e-005
128	7.569e-006	3.928e-006	9.974e-006	5.221e-006
256	1.340e-006	1.340e-006	2.482e-006	1.292e-006
512	3.102e-007	6.738e-007	5.919e-007	3.208e-007

Table 1: $\hat{u}^{n+1}$ and u_s^{n+n} are FEM solutions on $\hat{\mathcal{T}}^{n+1}$ and Shishkin mesh $\mathcal{T}_s^{n+n}$ for Example 6.1.

Let $\varepsilon = 10^{-10}$. Table 2 shows the accuracy of Q_i, the intersections of u^8 and u^{8+1}. Denote x- and y- coordinates of Q_i by $x(Q_i)$ and $y(Q_i)$, respectively. Note that Q_i has better accuracy than $\hat{u}^{8+1}$. The reason is yet to be discovered; see Table 2.

i	$x(Q_i)$	$\|y(Q_i) - u(x(Q_i))\|$	$\|y(Q_i) - u_I^8(x(Q_i))\|$
2	0.2499999996000000	7.499999579718697e-011	4.999999719812465e-011
3	0.2500000004000000	2.500008533523612e-011	8.326672684688674e-017
4	0.4999999992000000	3.500000012035542e-010	2.999999970665357e-010
5	0.5000000008000000	5.000011515932101e-011	1.110223024625157e-016
6	0.7499999988000000	6.625580639685325e-009	6.700580590379701e-009
7	0.7500000012000000	7.500006171667906e-011	1.110223024625157e-016

Table 2: errors at Q_i with $\varepsilon = 10^{-10}$ on $\mathcal{T}^8$ and $\mathcal{T}^{8+1}$ for Example 6.1.

Plotted in Figure 2 are the convergence curves in the maximum norm $\|u_I^{n+1} - \hat{u}^{n+1}\|_{\infty,[0,x_n]}$ for $\varepsilon = 10^{-5}$ and $\varepsilon = 10^{-10}$, respectively. They clearly indicate the convergence rate is proportional to n^{-2}. It verifies Remark 4.4; see Figure 2.

Example 6.2. We examine the problem of a reaction diffusion equation as another example of (1).

$$-\varepsilon u''(x) + u(x) = x, \quad u(0) = u(1) = 0. \tag{44}$$

The exact solution is

$$u(x) = x - \frac{e^{(x-1)/\sqrt{\varepsilon}} - e^{-(x+1)/\sqrt{\varepsilon}}}{1 - e^{-2/\sqrt{\varepsilon}}} \tag{45}$$

The exact solution $u(\cdot)$ has boundary layer at $x = 1$, and is nearly linear outside the boundary layer. Also, reaction diffusion equation has relatively stable matrix A compared with convection diffusion equation. Due to these reasons, the FEM solutions of (44) is better than the FEM solutions of (42).

For $\varepsilon = 10^{-10}$, we compute the FEM solution u^4 and u^{4+1} on the grid $\mathcal{T}^4$ and $\mathcal{T}^{4+1}$, where $\mathcal{T}^4$ is uniform mesh on $[0, 1]$ and $\mathcal{T}^{4+1}$ is modified by adding one point at the center of last interval; Figure 3-a.

By adding one point $\hat{s}_1 \in (x_n, 1)$ with $\hat{s}_1 - x_n = \sqrt{6\varepsilon}$ as in Lemma 4.1, we use new grid $\hat{\mathcal{T}}^{n+1}$, and denote its FEM solution as $\hat{u}^{4+1}$. As shown in Figure 3-b, $\hat{u}^{4+1}$ is almost overlapped with u_I^4, the interpolation of exact solution; see Figure 3-b.
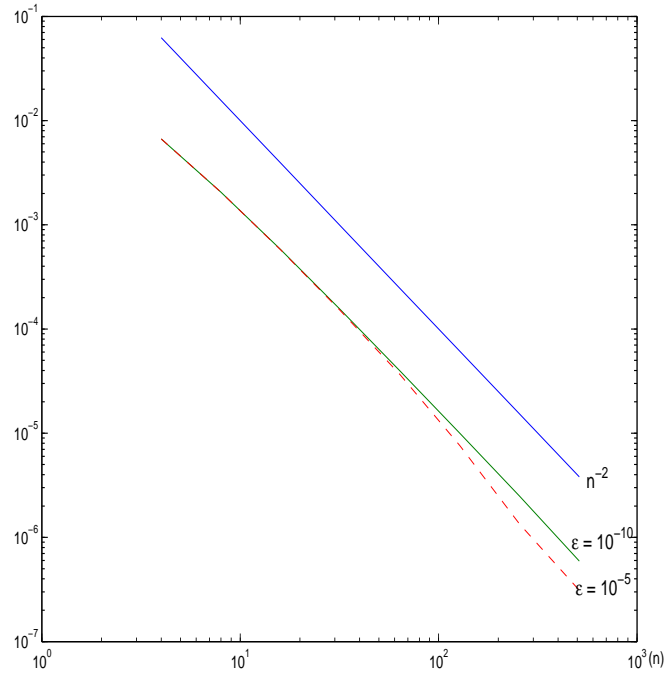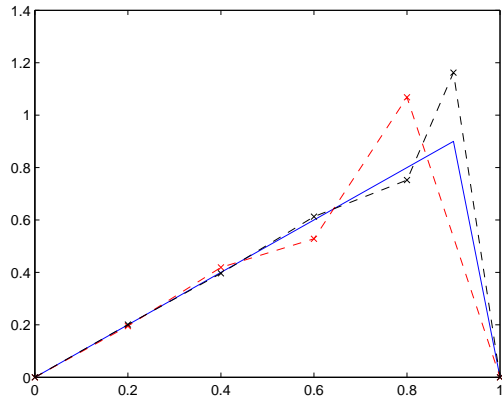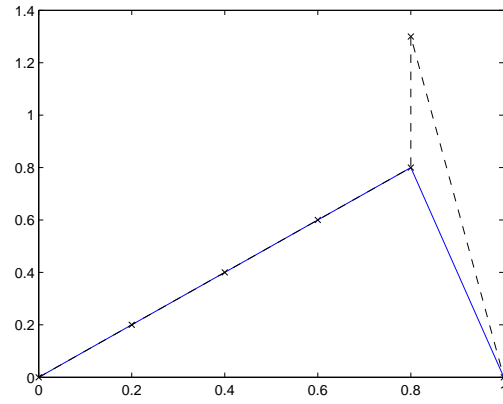
13

Figure 2: errors $\|u - \hat{u}^{n+1}\|_{\infty,[0,x_n]}$ with various n for Example 6.1.

(a) u^4 and u^{4+1}(dotted lines); u_I^{4+1}(solid line)

(b) $\hat{u}^{4+1}$(dotted line) and u_I^4(solid line)

Figure 3: FEMs with $\varepsilon = 10^{-10}$ for Example 6.2.

14

Let $\theta = \min\{\frac{1}{2}, \frac{\sqrt{\varepsilon}\ln 2n}{\sqrt{c}}\}$. We construct shishkin mesh $\mathcal{T}_s^{n+n}$ by dividing $[0, 1 - \theta]$ and $[1 - \theta, 1]$ into n equidistant subintervals. Table 3 present the errors of $\hat{u}^{n+1}$. Compared with u_s^{n+n}, the FEM solutions using Shishkin mesh $\mathcal{T}_s^{n+n}$, the errors are smaller and ε-uniform. We omit the convergence curve and error table of Q_i, since all those errors are within computer errors (around 10^{-14}).

	$\varepsilon = 10^{-5}$		$\varepsilon = 10^{-10}$	
n	$\|u_I^{n+1} - \hat{u}^{n+1}\|_{\infty,[0,x_n]}$	$\|u_I^{n+1} - u_s^{n+n}\|_{\infty,[0,x_n]}$	$\|u_I^{n+1} - \hat{u}^{n+1}\|_{\infty,[0,x_n]}$	$\|u_I^{n+1} - u_s^{n+n}\|_{\infty,[0,x_n]}$
4	1.665e-016	1.517e-004	1.110e-016	4.980e-007
8	1.110e-016	5.415e-005	2.220e-016	1.868e-007
16	2.220e-016	2.161e-005	3.331e-016	8.451e-008
32	2.220e-016	7.391e-006	3.331e-016	4.054e-008
64	3.331e-016	1.300e-006	5.551e-016	1.984e-008
128	4.441e-016	1.159e-009	5.551e-016	5.551e-016
256	2.459e-013	2.948e-007	6.661e-016	9.795e-009
512	5.440e-015	2.865e-007	7.772e-016	4.847e-009

Table 3: $\hat{u}^{n+1}$ and u_s^{n+n} are the FEM solutions on $\hat{\mathcal{T}}^{n+1}$ and Shishkin mesh $\mathcal{T}_s^{n+n}$ for Example 6.2.

Example 6.3. This example presents a demonstration of Corollary 3.5. Using the FEM, we aim to find the Green function (as a solution of)

$$-\varepsilon^2 u'' + u = \delta_\alpha, \quad u(0) = 0, u(1) = 0, \tag{46}$$

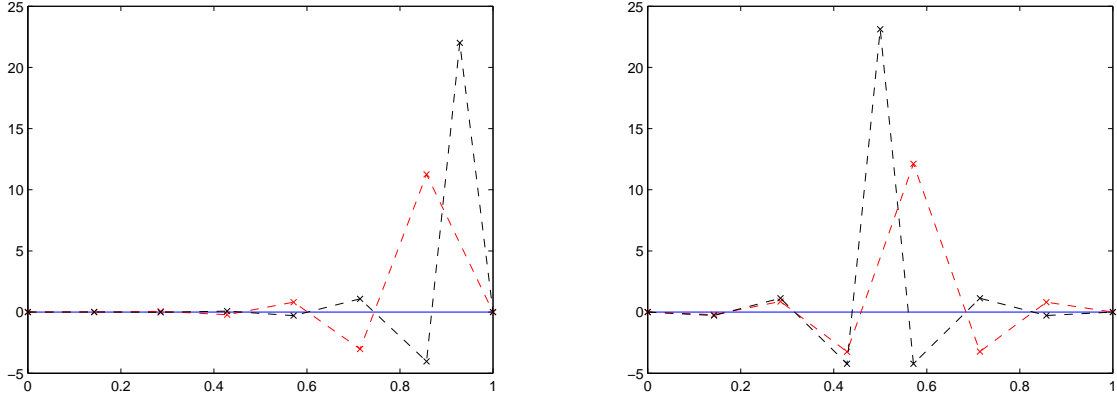where δ_α is delta function with peak at $\alpha \in (0, 1)$. Denote a function as

$$g(x) = \frac{e^{x/\varepsilon} - e^{-x/\varepsilon}}{e^{\alpha/\varepsilon} - e^{-\alpha/\varepsilon}}. \tag{47}$$

The exact solution of (46) is

$$u = \begin{cases} K_\alpha g(x) & 0 \le x \le \alpha \\ K_\alpha g\left(\frac{\alpha(1-x)}{1-\alpha}\right) & \alpha < x \le 1 \end{cases} \tag{48}$$

where $K_\alpha \simeq \alpha/\varepsilon$ is a constant depend on α and ε.

15

$\mathcal{T}^{6+1}$ used in Figure 4-a is modified from $\mathcal{T}^6$ by adding one point s_1 at the center of the last interval, while $\mathcal{T}^{6+1}$ used in Figure 4-b is modified by adding s_1 at the center of (x_3, x_4).

(a) u^6 and u^{6+1} (dotted lines) for $\frac{6}{7} < \alpha < 1$.   (b) u^6 and u^{6+1} (dotted lines) for $\frac{3}{7} < \alpha < \frac{4}{7}$.

Figure 4: FEMs with $\varepsilon = 10^{-5}$ for Example 6.3.

		$\frac{6}{7} < \alpha < 1$		$\frac{3}{7} < \alpha < \frac{4}{7}$
i	$x(Q_i)$	$\|y(Q_i) - u(x(Q_i))\|$	$x(Q_i)$	$\|y(Q_i) - u(x(Q_i))\|$
2	.1714	1.7347e-018	.1714	2.7756e-017
3	.3158	6.9389e-018	.3158	1.1102e-016
4	.4588	2.7756e-017	–	–
5	.6016	0	.6842	1.7764e-015
6	.7445	0	.8286	4.4409e-016

Table 4: errors at Q_i for $\varepsilon = 10^{-5}$ for Example 6.3.

7 Further Remarks

This paper is devoted to finite element methods for singularly perturbed boundary value problems. An interesting behavior is discovered: One can add arbitrary many points in

one of the grids, while the corresponding FEM solutions always have the common intersections $\{Q_i\}$ in all other intervals. Moreover, a practical and efficient ε-uniform mesh is developed. The FEM solution under this mesh can be viewed as a non-singularly perturbed BVP perturbation problem, and all general FEM error analysis can be applied.

In both Example 6.2 and Example 6.3, the errors are within computer error. However, the errors of Example 6.1 is visible errors relative to computer error. The main reason is the exact solution of Example 6.1 is almost quadratic, while our approximation is based on linear finite element space. To increase accuracy, one can generalize the results to the higher order finite element space. If the exact solution has several boundary layers, it can also be generalized to isolate each boundary layer.

Although the exact solution of Example 6.1 is nearly quadratic, the accuracy of intersections $\{Q_i\}$ is almost within computer error. We know $\hat{u}^{n+1}$ has the accuracy of $\hat{u}^{n+1+\infty}$, while $\{Q_i\}$ has the accuracy of $u^{n+\infty}$. The only difference of two is the interval $(x_n, \hat{s}_1)$ of width $O(\sqrt{\varepsilon})$ or $O(\sqrt{\varepsilon})$. In fact, this causes the error difference from Example 6.1. It might be interesting to discover the reason behind. It leads to the error analysis of non-quasiuniform meshes.

It is very challenged to generalize the idea to isolate boundary layer in higher dimensional cases. On the other hand, Lemma 5.1 provided a necessary and sufficient condition to verify the behavior of oscillation of specific FEM solution. However, it is not handy enough to explain why the oscillation behavior is common to FEM solutions. In general, the problem of determining in what cases the FEM solutions will or will not oscillate remains open.

References

[1] Towards optimization of methods for solving boundary value problems in the presence of boundary layers, *Zh. Vychisl. Mater. Mater. Fiz.*, 9:841-859, 1969, in Russian.

[2] Susanne C. Brenner, L. Ridgway Scott, *The mathematical Theory of Finite Element Methods*, Springer, 2002.

[3] Long Chen, Jinchao Xu, Stability and Accuracy of Adapted Finite Element Methods for Sigularly Perturbed Problems, *Numerische Mathematik*, preprint.

[4] E. P. Doolan, J. J. H. Miller, W. H. A. Schilders, *Uniform numerical methods for problems with initial and boundary layers,* Boole Press, Bublin, (1980).

[5] N. V. Kopteva. Uniform convergence with respect to a small parameter of a scheme with central difference on refining grids, *Comput. Math. Phys.*, **39** (1999), 1594-1610.

[6] N. V. Kopteva. Maximum norm a posteriori error estimates for a one-dimensional convection-diffusion problem, *SIAM J. Numeri. Anal.*, **39** (2001), 423-441.

[7] T. Linss. Layer-adapted meshes for convection-diffusion problems, *Comput. Methods Appl. Mech. Engrg.*, **192** (2003), 1061-1105.

[8] J. J. H. Miller, E. O'Riordan, and G. I. Shishkin. *Fitted Numerical Methods for Singular Perturbation Problems.* World Scientific, 1996.

[9] E. O'Riordan, M. Stynes, Auniformly accurate finite element method for a singularly perturbed one-dimensional reaction-diffusion problem, *Math. Comp.* **47** (1986), 555–570.

[10] Y. Qiu, D.M. Sloan, T. Tang, Numerical solution of perturbed two-point boundary value problem using equidistribution: analysis of convergence, *J. of Comput. and Appl. Math.*, **116** (2000), 121-143.

[11] H. G. Roos, M. Stynes, L. Tobiska, *Numerical methods for singularly purturbed differential equations: Convection-diffusion and flow problems* . Springer, 1996.

[12] H. G. Roos, Global uniformly convergent schemes for a singularly perturbed boundary value problem using patch base spline-functions, *J. Comput. Appl. Math.*, **29** (1990), 69–77.

[13] H. G. Roos, Layer-adapted grids for singular perturbation problems, *ZA-MMZ Angew Math Mech.*, **78-5** (1998), 291–309.

[14] G. I. Shishkin, *Grid approximation of sigulary perturbed elliptic and parabolic equations*, PhD thesis, Second doctorial thesis, Keldysh Institute, Moscow, 1990, in Russian.

[15] Zhimin Zhang, Finite elment superconvergence approximation for one-dimensional singularly perturbed problems, *Numer. Methods Partial Differential Equations*, **18** (2002), 374–395.